

# PointGPT: Auto-regressively Generative Pre-training from Point Clouds

Guangyan Chen<sup>1</sup> Meiling Wang<sup>1</sup> Yi Yang<sup>1</sup> Kai Yu<sup>1</sup> Li Yuan<sup>2</sup> \* Yufeng Yue<sup>1</sup> \*

<sup>1</sup> Beijing Institute of Technology

<sup>2</sup> Peking University

## Abstract

Large language models (LLMs) based on the generative pre-training transformer (GPT) [44] have demonstrated remarkable effectiveness across a diverse range of downstream tasks. Inspired by the advancements of the GPT, we present PointGPT, a novel approach that extends the concept of GPT to point clouds, addressing the challenges associated with disorder properties, low information density, and task gaps. Specifically, a point cloud auto-regressive generation task is proposed to pre-train transformer models. Our method partitions the input point cloud into multiple point patches and arranges them in an ordered sequence based on their spatial proximity. Then, an extractor-generator based transformer decoder [25], with a dual masking strategy, learns latent representations conditioned on the preceding point patches, aiming to predict the next one in an auto-regressive manner. Our scalable approach allows for learning high-capacity models that generalize well, achieving state-of-the-art performance on various downstream tasks. In particular, our approach achieves classification accuracies of 94.9% on the ModelNet40 dataset and 93.4% on the ScanObjectNN dataset, outperforming all other transformer models. Furthermore, our method also attains new state-of-the-art accuracies on all four few-shot learning benchmarks. Codes are available at <https://github.com/CGuangyan-BIT/PointGPT>.

## 1 Introduction

Point clouds are becoming widely adopted data structures in various application areas, such as autonomous driving and robotics, emphasizing the importance of acquiring informative and comprehensive 3D representations. However, current 3D-centric approaches [9; 38; 39; 56; 30] typically necessitate fully-supervised training from scratch, which entails labor-intensive human annotations. In natural language processing (NLP) and image analysis domains, self-supervised learning (SSL) [11; 18; 45; 5; 44] has emerged as a promising approach for acquiring latent representations without relying on annotations. Among these methods, the generative pre-training transformer (GPT) [44] has been particularly effective at learning representative features [7], where the task is to predict data in an auto-regressive manner. Due to its remarkable performance, we naturally ask the question: can the GPT be adapted to point clouds and serve as an effective 3D representation learner?

To answer this question, we exploit the GPT scheme for point cloud understanding. However, it is challenging to employ GPT on point clouds due to the following reasons: (I) Disorder properties. In contrast with the sequential arrangement of words in a sentence, a point cloud is a structure that lacks inherent order. To address this issue, point patches are arranged based on a geometric ordering, namely the Morton-order curve [34], which introduces sequential properties and preserves the local structures. (II) Information density differences. Languages are characterized by high information

\*Li Yuan and Yufeng Yue contributed equally to this study as co-corresponding authors.

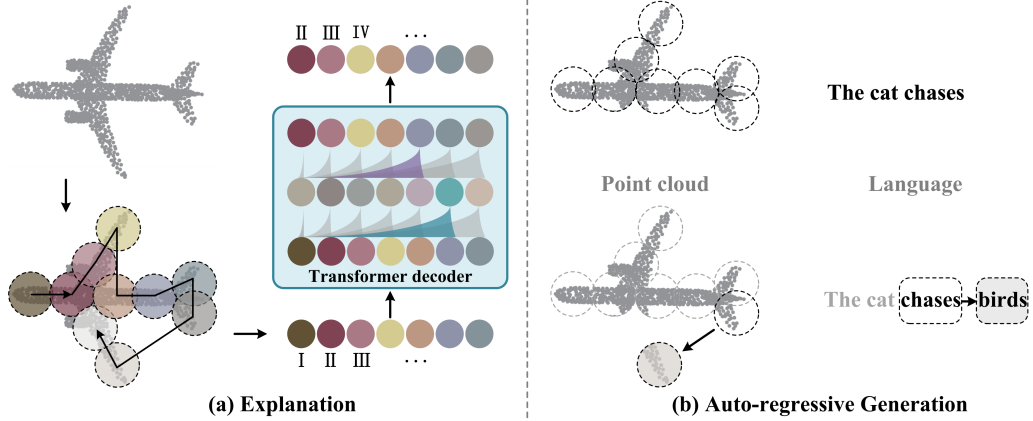


Figure 1: Illustration of our PointGPT. The transformer decoder is pre-trained to predict point patches in an auto-regressive manner. Such a design enables our method to predict patches without dedicated specifications and avoids positional information leakage, leading to improved generalization ability.

richness, therefore, the auto-regressive prediction task requires advanced language understanding. On the contrary, point clouds are natural signals with heavy redundancy, thereby the prediction task can be accomplished even without holistic comprehension. To address this disparity, a dual masking strategy is proposed, which additionally masks attending tokens for each token. This strategy effectively reduces redundancy and provides a challenging task that demands comprehensive understanding. (III) Gaps between generation and downstream tasks. Even though the model with a dual masking strategy exhibits sophisticated comprehension, the generation task primarily involves predicting individual points, which may result in the learned latent representations with a lower semantic level than downstream tasks. To mitigate this challenge, an extractor-generator architecture is introduced to the transformer decoder [25], such that the generation task is facilitated through the generator, thus enhancing the semantic level of the latent representations learned by the extractor.

Based on the above analysis, we propose a novel SSL framework for point clouds, called PointGPT. Specifically, our method partitions the input point cloud into multiple irregular point patches, which are subsequently organized using the Morton curve. Then, an extractor-generator based transformer decoder, with a dual masking strategy, processes the point patch sequences to learn latent representations conditioned on the unmasked preceding contents, and predicts the next point patches in an auto-regressive manner. Unlike recently developed masked point modeling approaches [64; 37; 66] that rely on positional information to specify reconstruction regions, resulting in the leakage of the overall object shape, our concise design, as illustrated in Figure 1, effectively circumvents the leakage of positional information and yields an enhanced generalization ability. Consequently, our PointGPT surpasses other single-modal SSL methods with comparable model sizes.

Inspired by the promising performance exhibited by our PointGPT, we endeavor to investigate its scaling property and push its performance limit further. However, a significant challenge arises due to the limited scale of the existing public point cloud datasets compared to NLP and images. This dataset size disparity introduces potential overfitting concerns. To alleviate this and fully unleash the power of PointGPT, a larger pre-training dataset is collected by mixing various point cloud datasets, such as ShapeNet [6] and S3DIS [3]. Moreover, a subsequent post-pre-training stage [55] is introduced, which involves performing supervised learning on the collected labeled dataset, enabling PointGPT to incorporate semantic information from multiple sources. Within this framework, our scaled models achieve state-of-the-art (SOTA) performance on various downstream tasks. In object classification tasks, our PointGPT achieves 94.9% accuracy on the ModelNet40 dataset and 93.4% accuracy on the ScanObjectNN dataset, outperforming all other transformer models. In few-shot learning tasks, our method also attains new SOTA performance on all four benchmarks.

Our main contributions can be summarized as follows: (I) A novel GPT scheme, termed PointGPT, is proposed for point cloud SSL. PointGPT leverages a point cloud auto-regressive generation task while mitigating positional information leakage, outperforming other single-modal SSL methods. (II) A dual masking strategy is proposed to create an effective generation task, and an extractor-generator transformer architecture is introduced to enhance the semantic level of the learned representations. These designs boost the performance of PointGPT on downstream tasks. (III) A post-pre-training

stage is introduced, and larger datasets are collected to facilitate the training of high-capacity models. With PointGPT, our scaled models achieve SOTA performance on various downstream tasks.

## 2 Related Work

### 2.1 Self-supervised Learning for NLP and Image Processing

Self-supervised learning has attracted significant attention in recent years, especially in the fields of NLP and image processing, owing to its ability to learn useful representations without labeled data. The core idea of SSL is to design a pretext task to learn the distribution of the given data, obtaining beneficial features for the subsequent supervised modeling tasks [21; 13]. Contrastive learning [8; 15; 63; 36; 32; 42; 49] has been a popular discriminative self-supervised approach in both NLP and image processing, with the goal of grouping similar samples closer and diverse samples further apart. However, generative SSL methods [4; 18; 7; 11; 47; 44] have recently achieved more competitive performance. BERT [11] utilizes a bidirectional transformer to process the randomly masked text and reconstruct the original context. ELMo [47] adopts bidirectional LSTM [19] and generates subsequent words from left to right given representations of the previous contents. The GPT [44] also utilizes the auto-regressive prediction approach, but it employs a unidirectional transformer architecture, and the model is fine-tuned by updating all pre-trained parameters. In the computer vision field, BEiT [4] and MAE [18] randomly mask input patches, and pre-train models to recover the masked patches in the pixel space. Image-GPT [7] trains a sequence transformer to auto-regressively predict pixels without incorporating knowledge concerning the 2D input structure, exhibiting promising representation learning capabilities after pre-training.

### 2.2 Self-supervised Learning for Point Cloud

The success of SSL in NLP and image processing has motivated researchers to develop SSL frameworks for point cloud representation learning. Among these methods, the contrastive methods [59; 67; 35; 20; 61] have been extensively investigated. DepthContrast [67] constructs augmented depth maps and performs an instance discrimination task for the extracted global features. Similarly, MVIF [20] introduces cross-modal and cross-view invariance constraints to achieve self-supervised modal- and view-invariant feature learning. Another line of work [40; 12; 60] is proposed to integrate cross-modal information and leverage knowledge transferred from language or image models for 3D learning. ACT [12] employs cross-modal auto-encoders as teacher models to acquire knowledge from other modalities. Different from these methods, our work attempts to learn the intrinsic properties of point clouds without relying on cross-modal information and teacher models. Most relevant to our work are generative methods [22; 1; 48; 37; 64; 66; 31], especially recently proposed masked point modeling methods [37; 64; 66; 31]. Point-MAE extends the MAE by randomly masking point patches and reconstructing masked regions. Point-M2AE additionally utilizes a hierarchical transformer architecture and designs a corresponding masking strategy. However, masked point modeling methods still suffer from overall object shape leakage, which limits their ability to effectively generalize to downstream tasks. In this paper, we exploit the auto-regressive pre-training for point clouds and address unique challenges associated with the properties of point clouds. Our concise design avoids positional information leakage, thereby enhancing the generalization ability.

## 3 PointGPT

Given a point cloud  $\mathbf{X} = \{x_1, x_2, \dots, x_M\} \subseteq \mathbb{R}^3$ , the overall pipeline of PointGPT during pre-training is illustrated in Fig. 2. The point cloud sequencer module is utilized to construct an ordered sequence of point patches. This is achieved by dividing the point cloud into irregular patches and arranging them in Morton order. The resulting sequence is then fed into the extractor to learn latent representations, and the generator predicts the subsequent point patches in an auto-regressive manner. After the pre-training stage, the generator is discarded, and the extractor without the use of a dual masking strategy, leverages the learned latent representations for downstream tasks.

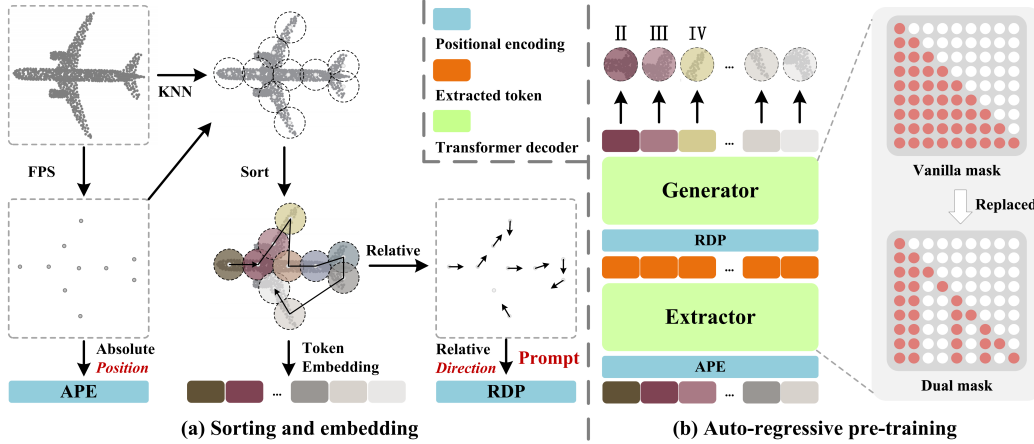


Figure 2: Overall architecture of our PointGPT. (a) The input point cloud is divided into multiple point patches, which are then sorted and arranged in an ordered sequence. (b) An extractor-generator based transformer decoder is employed along with a dual masking strategy for the auto-regressively prediction of the point patches. In this example, the additional mask of the dual masking strategy is applied to the same group of random tokens for better illustration purposes.

### 3.1 Point Cloud Sequencer

In the field of NLP, the GPT approach benefits from an easily accessible language vocabulary and the inherent ordered properties of words. In contrast, the point cloud domain lacks a predefined vocabulary, and a point cloud is a sparse structure that exhibits a characteristic of the disorder. To overcome these challenges and obtain an ordered point cloud sequence with each component unit capturing rich geometric information, a three-stage process consisting of point patch partitioning, sorting, and embedding is employed.

**Point patch partitioning:** Taking the inherent sparsity and disorder properties of point clouds into account, the input point clouds are processed by farthest point sampling (FPS) and the K-nearest neighbors (KNN) algorithms to obtain center points and point patches. Given a point cloud  $X$  with  $M$  points, we initially sample  $n$  center points  $C$  using FPS. Then, the KNN algorithm is utilized to construct  $n$  point patches  $P$  by selecting the  $k$  nearest points from  $X$  for each center point. In summary, the partitioning procedure is formulated as:

$$\begin{aligned} C &= \text{FPS}(X), \quad C \in \mathbb{R}^{n \times 3}; \\ P &= \text{KNN}(C, X), \quad P \in \mathbb{R}^{n \times k \times 3}. \end{aligned} \quad (1)$$

**Sorting:** To address the inherent disorder properties of point clouds, the obtained point patches are organized into a coherent sequence based on their center points. Concretely, the coordinates of the center points are encoded into one-dimensional space using Morton code [34], followed by sorting to determine the order  $\mathcal{O}$  of these center points. The point patches are then arranged in the same order. The sorted center points  $C^s$  and sorted point patches  $P^s$  are obtained as follows:

$$\begin{aligned} \mathcal{O} &= \text{argmax}(\text{MortonCode}(C)), \quad \mathcal{O} \in \mathbb{R}^{n \times 1}; \\ C^s, P^s &= C[\mathcal{O}], P[\mathcal{O}], \quad C^s \in \mathbb{R}^{n \times 3}, P^s \in \mathbb{R}^{n \times k \times 3}. \end{aligned} \quad (2)$$

**Embedding:** Following Point-MAE [37], a PointNet [38] network is employed to extract rich geometric information for each point patch. To facilitate training convergence, the normalized coordinates of each point are utilized with respect to its center point. Specifically, the sorted point patches  $P^s$  are embedded into  $D$ -dimensional tokens  $T$  as follows:

$$T = \text{PointNet}(P^s), \quad T \in \mathbb{R}^{n \times D}. \quad (3)$$

### 3.2 Transformer Decoder with a Dual Masking Strategy

A straightforward extension of the GPT [44] to point clouds can be achieved by utilizing the vanilla transformer decoder to auto-regressively predict point patches, followed by fine-tuning all pre-trained

parameters for downstream tasks. Nevertheless, this approach suffers from low-level semantics due to the limited information density of point clouds and the gaps between generation and downstream tasks. To address this issue, a dual masking strategy is proposed to facilitate comprehensive understanding of point clouds. Additionally, an extractor-generator transformer architecture is introduced, where the generator is more specialized for the generation task and is discarded after pre-training, enhancing the semantic level of the latent representations that are learned by the extractor.

**Dual masking strategy:** The vanilla masking strategy in the transformer decoder enables each token to receive information from all the preceding point tokens. To further encourage the learning of useful representations, the dual masking strategy is proposed, which additionally masks a proportion of the attending preceding tokens of each token during pre-training. The resulting dual mask  $M^d$  is illustrated in Fig. 2(b), the self-attention process with a dual masking strategy can be represented as:

$$\text{SelfAttention}(\mathbf{T}) = \text{softmax}\left(\frac{\mathbf{Q}\mathbf{K}^T}{\sqrt{D}} - (1 - M^d) \cdot \infty\right)\mathbf{V}. \quad (4)$$

where  $\mathbf{Q}, \mathbf{K}, \mathbf{V}$  are  $\mathbf{T}$  encoded with different weights for the  $D$  channels. The masked locations in  $M^d$  are set to 0, while the unmasked locations are set to 1.

**Extractor-generator:** Our extractor is composed entirely of transformer decoder blocks with a dual masking strategy, obtaining latent representations  $\mathcal{T}$ , where each point token only attends to the unmasked preceding tokens. Considering that point patches are represented in normalized coordinates, and global structures of point clouds are essential for point cloud understanding, sinusoidal positional encodings [53] (PE) are utilized to map the coordinates of the sorted center points  $\mathbf{C}^s$  to the absolute positional encoding (APE). Positional encodings are added to every transformer block to provide location information and incorporate global structural information.

The generator architecture is similar to the extractor architecture but contains fewer transformer blocks. It takes the extracted tokens  $\mathcal{T}$  as input and generates point tokens  $\mathbf{T}^g$  for the following prediction head. However, the patch order may be affected by the center point sampling process, inducing ambiguity when predicting the subsequent patches. This hinders the model from effectively learning meaningful point cloud representations. To address this issue, the directions relative to the subsequent point patches are provided in the generator, serving as prompts without revealing the locations of the masked patches and the overall object shapes of point clouds. The relative direction prompts  $RDP$  are formulated as:

$$RDP_i = \text{PE}((\mathbf{C}_{i+1}^s - \mathbf{C}_i^s) / \|\mathbf{C}_{i+1}^s - \mathbf{C}_i^s\|_2), i \in \{1, \dots, n'\}, \quad RDP \in \mathbb{R}^{n' \times D}, \quad (5)$$

where  $n' = n - 1$ . In summary, the procedure in the extractor-generator architecture is formulated as:

$$\begin{aligned} \mathcal{T} &= \text{Extractor}(\mathbf{T} + \text{APE}), \quad \mathcal{T} \in \mathbb{R}^{n \times D}; \\ \mathbf{T}^g &= \text{Generator}(\mathcal{T}_{1:n'} + RDP), \quad \mathbf{T}^g \in \mathbb{R}^{n' \times D}. \end{aligned} \quad (6)$$

**Prediction head.** The prediction head is utilized to predict the subsequent point patches in the coordinate space. It consists of a two-layer MLP with two fully connected (FC) layers and rectified linear unit (ReLU) activation. The prediction head projects tokens  $\mathbf{T}^g$  to vectors, where the number of output channels equals the total number of coordinates in a patch. Then, these vectors are reshaped to construct the predicted point patches  $\mathbf{P}^{pd}$ :

$$\mathbf{P}^{pd} = \text{Reshape}(\text{MLP}(\mathbf{T}^g)), \quad \mathbf{P}^{pd} \in \mathbb{R}^{n' \times k \times 3}. \quad (7)$$

### 3.3 Generation Target

The generation target for each point patch is to predict the coordinates of the points within the subsequent point patches. Given the predicted point patches  $\mathbf{P}^{pd}$ , as well as the ground-truth point patches  $\mathbf{P}^{gt}$ , which correspond to the last  $n'$  patches among the sorted point patches  $\mathbf{P}^s$ , the generation loss  $\mathcal{L}^g$  is formulated using the  $l_1$ -form and  $l_2$ -form of the Chamfer distance (CD) [14], denoted as  $\mathcal{L}_1^g$  and  $\mathcal{L}_2^g$ , respectively. Specifically, the generation loss is computed as  $\mathcal{L}^g = \mathcal{L}_1^g + \mathcal{L}_2^g$ . The  $l_n$ -form CD loss  $\mathcal{L}_n^g$ , with  $n \in \{1, 2\}$ , is defined as:

$$\mathcal{L}_n^g = \frac{1}{|\mathbf{P}^{pd}|} \sum_{a \in \mathbf{P}^{pd}} \min_{b \in \mathbf{P}^{gt}} \|a - b\|_n^n + \frac{1}{|\mathbf{P}^{gt}|} \sum_{b \in \mathbf{P}^{gt}} \min_{a \in \mathbf{P}^{pd}} \|a - b\|_n^n, \quad (8)$$

where  $|\mathbf{P}|$  is the cardinality of the set  $\mathbf{P}$  and  $\|a - b\|_n$  represents the  $L_n$  distance between  $a$  and  $b$ .

We additionally find that incorporating the generation task into the fine-tuning process as an auxiliary objective can accelerate training convergence and improve the generalization ability of supervised models. This approach yields enhanced performance on downstream tasks, which is in line with the GPT [44]. Specifically, we optimize the following objective during the fine-tuning stage:  $\mathcal{L}^f = \mathcal{L}^d + \lambda \times \mathcal{L}^g$ , where  $\mathcal{L}^d$  represents the loss for the downstream task,  $\mathcal{L}^g$  represents the generation loss as previously defined, and the parameter  $\lambda$  balances the contribution of each loss term.

### 3.4 Post-Pre-training

Current point cloud SSL methods directly fine-tune pre-trained models on the target dataset, which may result in potential overfitting due to the limited semantic supervision information [55]. To alleviate this issue and facilitate training of high-capacity models, we adopt the intermediate fine-tuning strategy [55; 4; 27] and introduce a post-pre-training stage for PointGPT. In this stage, a labeled hybrid dataset is leveraged (Sec. 4.1), which collects and aligns multiple point cloud datasets with labels. By conducting supervised training on this dataset, semantic information is effectively incorporated from diverse sources. Subsequently, fine-tuning is performed on the target dataset to transfer the learned general semantics to task-specific knowledge.

## 4 Experiments

This section begins by presenting the implementation and our pre-training setups. Subsequently, the effectiveness of our pre-trained models is evaluated across a range of downstream tasks. Finally, ablation studies are conducted to analyze the main properties of our PointGPT.

### 4.1 Implementation and Pre-training Setups

**Models:** Following previous studies [37; 64], PointGPT is trained employing the ViT-S configuration [65] for the extractor module, referred to as PointGPT-S. Additionally, we investigate the high-capacity models by scaling the extractor to the ViT-B and ViT-L configurations, denoted as PointGPT-B and PointGPT-L, respectively. More details can be found in the appendix.

**Data:** PointGPT-S is pre-trained on the ShapeNet [6] dataset without subsequent post-pre-training. This is in line with the previous SSL methods [37; 64; 66; 24] to allow for a direct comparison with these prior approaches. ShapeNet contains over 50,000 unique 3D models across 55 object categories. Additionally, two datasets are collected to support the training of high-capacity PointGPT models (PointGPT-B and PointGPT-L): (I) an unlabeled hybrid dataset (UHD) for self-supervised pre-training, which collects point clouds from various datasets [50; 33; 6; 51; 3; 58; 16], such as ShapeNet [6], S3DIS [3] for indoor scenes, and Semantic3D [16] for outdoor scenes, etc. In total, the UHD contains approximately 300K point clouds; (II) a labeled hybrid dataset (LHD) for supervised post-pre-training, which aligns the label semantics of different datasets [50; 33; 6; 51; 3; 58], with 87 categories and approximately 200K point clouds in total. Further details are provided in the appendix.





**Pre-training setups:** The input point clouds are obtained by sampling 1024 points from each raw point cloud. Afterward, each point cloud is partitioned into 64 point patches, with each patch consisting of 32 points. The PointGPT model is pre-trained for 300 epochs using an AdamW optimizer [29] with a batch size of 128, an initial learning rate of 0.001, and a weight decay of 0.05. Additionally, based on our empirical results, cosine learning rate decay [28] is employed.

### 4.2 Downstream Tasks

To demonstrate the performance of our method on different downstream tasks, we conduct experiments involving object classification on real-world and clean object datasets, few-shot learning, and part segmentation. The performance of PointGPT is evaluated using three different model capacities: PointGPT-S, which is pre-trained on the ShapeNet dataset without post-pre-training; and PointGPT-B and PointGPT-L, which undergo both pre-training and post-pre-training stages on the collected hybrid datasets. The impact of post-pre-training is further investigated and discussed in the appendix.

**Object classification on a real-world dataset:** The performance of the proposed method on a real-world dataset is an important indicator of its practical applicability. Therefore, the pre-trained models are transferred to the ScanObjectNN dataset [52], which contains approximately 15,000

Table 1: Classification results on ScanObjectNN and ModelNet40 datasets. All results are expressed as percentages. Specifically, three variants are evaluated on the ScanObjectNN dataset. Additionally, The accuracy obtained on the ModelNet40 dataset is reported for both 1k and 8k points. The symbols ● and ● denote **larger pre-training dataset** and **post-pre-training stage**, respectively.

Methods	Reference	ScanObjectNN			ModelNet40	
		OBJ_BG	OBJ_ONLY	PB_T50_RS	1k P	8k P
Supervised Learning Only						
PointNet [38]	CVPR 2017	73.3	79.2	68.0	89.2	90.8
DGCNN [56]	TOG 2019	82.8	86.2	78.1	92.9	-
PointCNN [23]	Neurips 2018	86.1	85.5	78.5	92.2	-
GBNet [43]	TMM 2021	-	-	81.0	93.8	-
MVTN [17]	ICCV 2021	92.6	92.3	82.8	93.8	-
PointMLP [30]	ICLR 2022	-	-	85.4	94.5	-
PointNeXt [41]	Neurips 2022	-	-	87.7	94.0	-
P2P-RN101 [57]	Neurips 2022	-	-	87.4	93.1	-
P2P-HorNet [57]	Neurips 2022	-	-	89.3	94.0	-
with Self-Supervised Representation Learning						
Point-BERT [64]	CVPR 2022	87.4	88.1	83.1	93.2	93.8
MaskPoint [24]	ECCV 2022	89.3	88.1	84.3	93.8	-
Point-MAE [37]	ECCV 2022	90.0	88.2	85.2	93.8	94.0
Point-M2AE [66]	Neurips 2022	91.2	88.8	86.4	94.0	-
PointGPT-S	-	91.6	90.0	86.9	94.0	94.2
PointGPT-B  	-	95.8	95.2	91.9	94.4	94.6
PointGPT-L  	-	97.2	96.6	93.4	94.7	94.9
Methods using cross-modal information and teacher models						
ACT [12]	ICLR 2023	93.3	91.9	88.2	93.7	94.0
PointMLP+ULIP [60]	CVPR 2023	-	-	89.4	94.5	94.7
ReCon [40]	ICML 2023	95.4	93.6	91.3	94.5	94.7

objects extracted from real-world indoor scans. The experiments are conducted under three different settings, OBJ-BG, OBJ-ONLY, and PB-T50-RS. The results are presented in Table 1, our PointGPT-S, which has similar capacities and training data to previous methods like Point-MAE, outperforms other single-modal SSL methods. Furthermore, even when compared to Recon and ULIP, which utilize cross-modal information and teacher models, our scaled PointGPT-B model achieves superior performance, and PointGPT-L achieves accuracy improvements of at least 1.8%.

**Object classification on a clean objects dataset:** The pre-trained models are evaluated on the ModelNet40 dataset [58], which includes 12,311 clean 3D CAD models, covering 40 categories. To conduct fair comparisons, the standard voting method [26] is used during testing, and the input point clouds exclusively contain coordinate information, without additional normal information provided. The experimental results are presented in Table 1, our PointGPT-S surpasses other single-modal SSL methods. Even in comparison with Recon and ULIP, our PointGPT-L achieves superior performance.

**Few-shot learning:** To intuitively demonstrate the generalization ability of our method, few-shot learning experiments are conducted on the ModelNet40 dataset without the post-pre-training stage. Following the protocols of previous studies [37; 64; 66], the few-shot learning experiments consist of four distinct tests, employing  $w$ -way,  $s$ -shot setting. Specifically,  $w \in \{5, 10\}$  represents the number of randomly selected classes, and  $s \in \{10, 20\}$  denotes the number of randomly sampled objects for each selected class. Each test is conducted with 10 independent trials. The results, as shown in Table 2, indicate that our method outperforms other methods in all tests, particularly in the 10-shot tests. This demonstrates the ability of PointGPT in acquiring knowledge for new tasks, even under the constraints of limited training data.

**Part segmentation:** The representation learning capability of our method is evaluated on the ShapeNetPart [62] dataset, which consists of 16881 objects across 16 categories. The point clouds are sampled into 2048 points, and the segmentation head [37] concatenates the extracted features from layers  $\frac{1 \times td}{3}$ ,  $\frac{2 \times td}{3}$ , and  $\frac{3 \times td}{3}$  of the extractor transformer blocks, with  $td$  representing the depth of the extractor. Subsequently, average pooling, max pooling, and upsampling are utilized to generate

Table 2: Few-shot classification results on the ModelNet40 dataset. In each experimental setting, 10 independent trials are conducted, and the mean accuracy (%) is reported with its standard deviation. Symbol • denotes **larger pre-training dataset**, and the **post-pre-training stage** • is excluded.

Methods	Reference	5-way		10-way	
		10-shot	20-shot	10-shot	20-shot
DGCNN [56]	TOG 2019	31.6±2.8	40.8±4.6	19.9±2.1	16.9±1.5
OcCo [54]	ICCV 2021	90.6±2.8	92.5±1.9	82.9±1.3	86.5±2.2
<i>with Self-Supervised Representation Learning</i>					
Point-BERT [64]	CVPR 2022	94.6±3.1	96.3±2.7	91.0±5.4	92.7±5.1
MaskPoint [24]	ECCV 2022	95.0±3.7	97.2±1.7	91.4±4.0	93.4±3.5
Point-MAE [37]	ECCV 2022	96.3±2.5	97.8±1.8	92.6±4.1	95.0±3.0
Point-M2AE [66]	Neurips 2022	96.8±1.8	98.3±1.4	92.3±4.5	95.0±3.0
<b>PointGPT-S</b>	-	<b>96.8±2.0</b>	<b>98.6±1.1</b>	<b>92.6±4.6</b>	<b>95.2±3.4</b>
<b>PointGPT-B •</b>	-	<b>97.5±2.0</b>	<b>98.8±1.0</b>	<b>93.5±4.0</b>	<b>95.8±3.0</b>
<b>PointGPT-L •</b>	-	<b>98.0±1.9</b>	<b>99.0±1.0</b>	<b>94.1±3.3</b>	<b>96.1±2.8</b>
Methods using cross-modal information and teacher models					
ACT [12]	ICLR 2023	96.8±2.3	98.0±1.4	93.3±4.0	95.6±2.8
ReCon [40]	ICML 2023	97.3±1.9	98.9±1.2	93.3±3.9	95.8±3.0

Table 3: Part segmentation results on the ShapeNetPart dataset. The mean intersection over union (mIoU) is reported across all classes (Cls.) and all instances (Inst.). Symbols • and • denote **larger pre-training dataset** and **post-pre-training stage**, respectively.

Methods	Reference	Cls. mIoU(%)	Inst. mIoU(%)
PointNet [38]	CVPR 2017	80.4	83.7
PointNet++ [39]	Neurips 2017	81.9	85.1
DGCNN [56]	TOG 2019	82.3	85.2
PointMLP [30]	ICLR 2022	84.6	86.1
<i>with Self-Supervised Representation Learning</i>			
PointContrast [59]	ECCV 2020	-	85.1
CrossPoint [2]	CVPR 2022	-	85.5
Point-BERT [64]	CVPR 2022	84.1	85.6
Point-MAE [37]	ECCV 2022	-	86.1
<b>PointGPT-S</b>	-	<b>84.1</b>	<b>86.2</b>
<b>PointGPT-B • •</b>	-	<b>84.5</b>	<b>86.5</b>
<b>PointGPT-L • •</b>	-	<b>84.8</b>	<b>86.6</b>
Methods using cross-modal information and teacher models			
ACT [12]	ICLR 2023	84.7	86.1
ReCon [40]	ICML 2023	84.8	86.4

features for each point and an MLP is applied for label prediction. The experimental results, displayed in Table 3, demonstrate the superior performance of our PointGPT-L compared to all other methods.

### 4.3 Ablation Studies

Comprehensive ablation studies are conducted to investigate the fundamental designs of our PointGPT model. The impacts of these designs are evaluated by reporting the accuracy achieved by fine-tuning the model on the ModelNet40 dataset for object classification. To provide an intuitive representation of the results, ablation studies are conducted using the PointGPT-S model, which is pre-trained on the ShapeNet dataset and directly fine-tuned on the target dataset without post-pre-training.

**Generator:** Table 4(a) investigates the effect of varying the generator depth. The results demonstrate that the extractor-generator architecture facilitates the learning of strong semantic representations, particularly when combined with a deep generator, resulting in improved performance overall. However, due to the computational complexity associated with the deep generator, a depth of 4 is selected as the default setting for the generator.

**Generation targets:** The generation objective is essential for enabling the model to learn the intrinsic characteristics of the given data. Table 4(b) exhibits four distinct generation targets, which can



Table 4: Ablation experiments with PointGPT-S pertaining on the ShapeNet dataset. The fine-tuned accuracy (%) achieved without post-pre-training is reported. Default settings are marked in gray.

(a) Generator depth.		(b) Generation targets.		(c) Generation during fine-tuning.			
Blocks	Acc.	Targets	Acc.	Coef.	Acc.		
0	93.85 %	Coordinates	94.21 %	0	94.01%		
2	94.08 %	FPFH	94.13 %	1	94.15%		
4	94.21 %	PointNet	94.31 %	3	94.21%		
6	94.24 %	DGCNN	94.35 %	5	94.05%		
(d) Generation loss.		(e) Relative direction prompts.		(f) Dual masking strategy.			
Loss	Acc.	Case	Acc.	Ratio	Acc.	Ratio	Acc.
CD $l1$	93.66%	None	93.69%	0	93.68%	5	94.01%
CD $l2$	94.13%	Absolute position	94.06%	1	93.70%	7	94.21%
CD $l1+l2$	94.21%	Relative direction	94.21%	3	93.85%	9	93.66%

be categorized into two groups: one-stage targets that can be directly obtained, including point coordinates and FPFH [46], and two-stage targets that are extracted by a trained deep network, including PointNet [38] and the DGCNN [56]. The experimental results indicate that the use of handcrafted FPFH features leads to underperformance, which may be attributed to the overfitting of low-level geometric features. The variants with two-stage targets outperform the variant with point coordinate targets. However, the pre-training and inference processes of the teacher model inevitably incur an additional computational cost.

**Generation task in the fine-tuning stage:** The generation task is included as an auxiliary objective during the fine-tuning stage. Table 4(c) presents the obtained results when varying the coefficient  $\lambda$  of the generation loss in the fine-tuning loss. The results signify that this auxiliary objective serves as a regularization term and improves the generalization ability of supervised models. Furthermore, the results suggest that as the coefficient increases, the accuracy achieved in the classification task exhibits an increasing trend followed by a decreasing trend, reaching its highest value when  $\lambda = 3$ .

**Generation loss:** Table 4(d) presents the performance of variants using different generation loss functions, including the  $l1$ -form CD loss, the  $l2$ -form CD loss, and the combination of both the  $l1$ - and  $l2$ -forms CD loss. The results demonstrate that the combination of the  $l1$ - and  $l2$ -forms achieves superior performance. We analyze that the  $l2$ -form is more effective in guiding the network toward convergence and the  $l1$ -form has better sparsity, thus the combination of both forms is more effective.

**Relative direction prompts:** The effect of utilizing relative direction prompts is analyzed in Table 4(e). The variant utilizing relative direction prompts outperforms the variants using absolute positional encoding and excluding positional encoding. We hypothesize that this improvement stems from the ability of relative direction prompts to prevent the model from overfitting to the patch order, thus enhancing the performance of PointGPT in downstream tasks.

**Dual masking strategy:** We conduct an analysis on the impact of the dual masking strategy and search for the proper mask ratio, as shown in Table 4(f). Decreasing the mask ratio to 0 corresponds to employing the vanilla masking strategy. The results indicate that both excessive and insufficient masking ratios lead to a decline in performance. The experimental results demonstrate that the dual masking strategy is effective in promoting beneficial representation learning and enhancing the generalization ability of the pre-trained model.

## 5 Conclusion

In this paper, we present PointGPT, a novel approach that extends the GPT concept to point clouds, addressing the challenges associated with disorder properties, information density differences, and gaps between the generation and downstream tasks. Unlike recently proposed self-supervised masked point modeling approaches, our method avoids overall object shape leakage, attaining improved generalization ability. Additionally, we explore a high-capacity model training process and collect

hybrid datasets for pre-training and post-pre-training. The effectiveness and strong generalization capabilities of our approach are verified on various tasks, indicating that our PointGPT outperforms other single-modal methods with similar model capacities. Furthermore, our scaled models achieve SOTA performance on various downstream tasks, without the need for cross-modal information and teacher models. Despite the promising performance exhibited by PointGPT, the data and model scales explored for PointGPT remain several orders of magnitude smaller than those in NLP [5; 10] and image processing [65; 27] domains. Our aspiration is that our research can stimulate further exploration in this direction and narrow the gaps between point clouds and these domains.

## References

- [1] Panos Achlioptas, Olga Diamanti, Ioannis Mitliagkas, and Leonidas Guibas. Learning representations and generative models for 3d point clouds. In *International conference on machine learning*, pages 40–49. PMLR, 2018.
- [2] Mohamed Afham, Isuru Dissanayake, Dinithi Dissanayake, Amaya Dharmasiri, Kanchana Thilakarathna, and Ranga Rodrigo. Crosspoint: Self-supervised cross-modal contrastive learning for 3d point cloud understanding. In *Proceedings of the IEEE/CVF Conference on Computer Vision and Pattern Recognition*, pages 9902–9912, 2022.
- [3] Iro Armeni, Ozan Sener, Amir R Zamir, Helen Jiang, Ioannis Brilakis, Martin Fischer, and Silvio Savarese. 3d semantic parsing of large-scale indoor spaces. In *Proceedings of the IEEE conference on computer vision and pattern recognition*, pages 1534–1543, 2016.
- [4] Hangbo Bao, Li Dong, Songhao Piao, and Furu Wei. Beit: Bert pre-training of image transformers. *arXiv preprint arXiv:2106.08254*, 2021.
- [5] Tom B Brown, Benjamin Mann, Nick Ryder, Melanie Subbiah, Jared Kaplan, Prafulla Dhariwal, Arvind Neelakantan, Pranav Shyam, Girish Sastry, Amanda Askell, et al. Language models are few-shot learners. *arXiv preprint arXiv:2005.14165*, 2020.
- [6] Angel X Chang, Thomas Funkhouser, Leonidas Guibas, Pat Hanrahan, Qixing Huang, Zimo Li, Silvio Savarese, Manolis Savva, Shuran Song, Hao Su, et al. Shapenet: An information-rich 3d model repository. *arXiv preprint arXiv:1512.03012*, 2015.
- [7] Mark Chen, Alec Radford, Rewon Child, Jeffrey Wu, Heewoo Jun, David Luan, and Ilya Sutskever. Generative pretraining from pixels. In *International conference on machine learning*, pages 1691–1703. PMLR, 2020.
- [8] Ting Chen, Simon Kornblith, Mohammad Norouzi, and Geoffrey Hinton. A simple framework for contrastive learning of visual representations. In *International conference on machine learning*, pages 1597–1607. PMLR, 2020.
- [9] Christopher Choy, JunYoung Gwak, and Silvio Savarese. 4d spatio-temporal convnets: Minkowski convolutional neural networks. In *Proceedings of the IEEE/CVF conference on computer vision and pattern recognition*, pages 3075–3084, 2019.
- [10] Navneet Dalal and Bill Triggs. Histograms of oriented gradients for human detection. In *2005 IEEE computer society conference on computer vision and pattern recognition (CVPR’05)*, volume 1, pages 886–893. Ieee, 2005.
- [11] Jacob Devlin, Ming-Wei Chang, Kenton Lee, and Kristina Toutanova. Bert: Pre-training of deep bidirectional transformers for language understanding. *arXiv preprint arXiv:1810.04805*, 2018.
- [12] Runpei Dong, Zekun Qi, Linfeng Zhang, Junbo Zhang, Jianjian Sun, Zheng Ge, Li Yi, and Kaisheng Ma. Autoencoders as cross-modal teachers: Can pretrained 2d image transformers help 3d representation learning? *arXiv preprint arXiv:2212.08320*, 2022.
- [13] Dumitru Erhan, Aaron Courville, Yoshua Bengio, and Pascal Vincent. Why does unsupervised pre-training help deep learning? In *Proceedings of the thirteenth international conference on artificial intelligence and statistics*, pages 201–208. JMLR Workshop and Conference Proceedings, 2010.
- [14] Haoqiang Fan, Hao Su, and Leonidas J Guibas. A point set generation network for 3d object reconstruction from a single image. In *Proceedings of the IEEE conference on computer vision and pattern recognition*, pages 605–613, 2017.
- [15] Ian Goodfellow, Jean Pouget-Abadie, Mehdi Mirza, Bing Xu, David Warde-Farley, Sherjil Ozair, Aaron Courville, and Yoshua Bengio. Generative adversarial networks. *Communications of the ACM*, 63(11):139–144, 2020.
- [16] Timo Hackel, Nikolay Savinov, Lubor Ladicky, Jan D Wegner, Konrad Schindler, and Marc Pollefeys. Semantic3d. net: A new large-scale point cloud classification benchmark. *arXiv preprint arXiv:1704.03847*, 2017.
- [17] Abdullah Hamdi, Silvio Giancola, and Bernard Ghanem. Mvtn: Multi-view transformation network for 3d shape recognition. In *Proceedings of the IEEE/CVF International Conference on Computer Vision*, pages 1–11, 2021.
- [18] Kaiming He, Xinlei Chen, Saining Xie, Yanghao Li, Piotr Dollár, and Ross Girshick. Masked autoencoders are scalable vision learners. In *Proceedings of the IEEE/CVF Conference on Computer Vision and Pattern Recognition*, pages 16000–16009, 2022.

- [19] Sepp Hochreiter and Jürgen Schmidhuber. Long short-term memory. *Neural computation*, 9(8):1735–1780, 1997.
- [20] Longlong Jing, Yucheng Chen, Ling Zhang, Mingyi He, and Yingli Tian. Self-supervised modal and view invariant feature learning. *arXiv preprint arXiv:2005.14169*, 2020.
- [21] Julia A Lasserre, Christopher M Bishop, and Thomas P Minka. Principled hybrids of generative and discriminative models. In *2006 IEEE Computer Society Conference on Computer Vision and Pattern Recognition (CVPR’06)*, volume 1, pages 87–94. IEEE, 2006.
- [22] Jiaxin Li, Ben M Chen, and Gim Hee Lee. So-net: Self-organizing network for point cloud analysis. In *Proceedings of the IEEE conference on computer vision and pattern recognition*, pages 9397–9406, 2018.
- [23] Yangyan Li, Rui Bu, Mingchao Sun, Wei Wu, Xinhan Di, and Baoquan Chen. Pointcnn: Convolution on x-transformed points. *Advances in neural information processing systems*, 31:820–830, 2018.
- [24] Haotian Liu, Mu Cai, and Yong Jae Lee. Masked discrimination for self-supervised learning on point clouds. In *Computer Vision–ECCV 2022: 17th European Conference, Tel Aviv, Israel, October 23–27, 2022, Proceedings, Part II*, pages 657–675. Springer, 2022.
- [25] Peter J Liu, Mohammad Saleh, Etienne Pot, Ben Goodrich, Ryan Sepassi, Lukasz Kaiser, and Noam Shazeer. Generating wikipedia by summarizing long sequences. *arXiv preprint arXiv:1801.10198*, 2018.
- [26] Yongcheng Liu, Bin Fan, Shiming Xiang, and Chunhong Pan. Relation-shape convolutional neural network for point cloud analysis. In *Proceedings of the IEEE/CVF conference on computer vision and pattern recognition*, pages 8895–8904, 2019.
- [27] Ze Liu, Han Hu, Yutong Lin, Zhuliang Yao, Zhenda Xie, Yixuan Wei, Jia Ning, Yue Cao, Zheng Zhang, Li Dong, et al. Swin transformer v2: Scaling up capacity and resolution. In *Proceedings of the IEEE/CVF conference on computer vision and pattern recognition*, pages 12009–12019, 2022.
- [28] I Loshchilov and F Hutter. Stochastic gradient descent with warm restarts. In *Proceedings of the 5th Int. Conf. Learning Representations*, pages 1–16, 2016.
- [29] Ilya Loshchilov and Frank Hutter. Decoupled weight decay regularization. *arXiv preprint arXiv:1711.05101*, 2017.
- [30] Xu Ma, Can Qin, Haoxuan You, Haoxi Ran, and Yun Fu. Rethinking network design and local geometry in point cloud: A simple residual mlp framework. *arXiv preprint arXiv:2202.07123*, 2022.
- [31] Chen Min, Dawei Zhao, Liang Xiao, Yiming Nie, and Bin Dai. Voxel-mae: Masked autoencoders for pre-training large-scale point clouds. *arXiv preprint arXiv:2206.09900*, 2022.
- [32] Ishan Misra and Laurens van der Maaten. Self-supervised learning of pretext-invariant representations. In *Proceedings of the IEEE/CVF conference on computer vision and pattern recognition*, pages 6707–6717, 2020.
- [33] Kaichun Mo, Shilin Zhu, Angel X Chang, Li Yi, Subarna Tripathi, Leonidas J Guibas, and Hao Su. Partnet: A large-scale benchmark for fine-grained and hierarchical part-level 3d object understanding. In *Proceedings of the IEEE/CVF conference on computer vision and pattern recognition*, pages 909–918, 2019.
- [34] Guy M Morton. A computer oriented geodetic data base and a new technique in file sequencing. 1966.
- [35] KL Navaneet, Ansu Mathew, Shashank Kashyap, Wei-Chih Hung, Varun Jampani, and R Venkatesh Babu. From image collections to point clouds with self-supervised shape and pose networks. In *Proceedings of the IEEE/CVF Conference on Computer Vision and Pattern Recognition*, pages 1132–1140, 2020.
- [36] Aaron van den Oord, Yazhe Li, and Oriol Vinyals. Representation learning with contrastive predictive coding. *arXiv preprint arXiv:1807.03748*, 2018.
- [37] Yatian Pang, Wenxiao Wang, Francis EH Tay, Wei Liu, Yonghong Tian, and Li Yuan. Masked autoencoders for point cloud self-supervised learning. *arXiv preprint arXiv:2203.06604*, 2022.
- [38] Charles R Qi, Hao Su, Kaichun Mo, and Leonidas J Guibas. Pointnet: Deep learning on point sets for 3d classification and segmentation. In *Proceedings of the IEEE conference on computer vision and pattern recognition*, pages 652–660, 2017.
- [39] Charles R Qi, Li Yi, Hao Su, and Leonidas J Guibas. Pointnet++: Deep hierarchical feature learning on point sets in a metric space. *arXiv preprint arXiv:1706.02413*, 2017.
- [40] Zekun Qi, Runpei Dong, Guofan Fan, Zheng Ge, Xiangyu Zhang, Kaisheng Ma, and Li Yi. Contrast with reconstruct: Contrastive 3d representation learning guided by generative pretraining. *arXiv preprint arXiv:2302.02318*, 2023.
- [41] Guocheng Qian, Yuchen Li, Houwen Peng, Jinjie Mai, Hasan Hammoud, Mohamed Elhoseiny, and Bernard Ghanem. Pointnext: Revisiting pointnet++ with improved training and scaling strategies. *Advances in Neural Information Processing Systems*, 35:23192–23204, 2022.
- [42] Rui Qian, Tianjian Meng, Boqing Gong, Ming-Hsuan Yang, Huisheng Wang, Serge Belongie, and Yin Cui. Spatiotemporal contrastive video representation learning. In *Proceedings of the IEEE/CVF Conference on Computer Vision and Pattern Recognition*, pages 6964–6974, 2021.
- [43] Shi Qiu, Saeed Anwar, and Nick Barnes. Geometric back-projection network for point cloud classification. *IEEE Transactions on Multimedia*, 24:1943–1955, 2021.
- [44] Alec Radford, Karthik Narasimhan, Tim Salimans, and Ilya Sutskever. Improving language understanding by generative pre-training. 2018.
- [45] Alec Radford, Jeffrey Wu, Rewon Child, David Luan, Dario Amodei, Ilya Sutskever, et al. Language models are unsupervised multitask learners. *OpenAI blog*, 1(8):9, 2019.
- [46] Radu Bogdan Rusu, Nico Blodow, and Michael Beetz. Fast point feature histograms (fpfh) for 3d registration. In *2009 IEEE international conference on robotics and automation*, pages 3212–3217. IEEE,

- 2009.
- [47] Justyna Sarzynska-Wawer, Aleksander Wawer, Aleksandra Pawlak, Julia Szymanowska, Izabela Stefaniak, Michal Jarkiewicz, and Lukasz Okruszek. Detecting formal thought disorder by deep contextualized word representations. *Psychiatry Research*, 304:114135, 2021.
  - [48] Jonathan Sauder and Bjarne Sievers. Self-supervised deep learning on point clouds by reconstructing space. *Advances in Neural Information Processing Systems*, 32, 2019.
  - [49] Pierre Sermanet, Corey Lynch, Yevgen Chebotar, Jasmine Hsu, Eric Jang, Stefan Schaal, Sergey Levine, and Google Brain. Time-contrastive networks: Self-supervised learning from video. In *2018 IEEE international conference on robotics and automation (ICRA)*, pages 1134–1141. IEEE, 2018.
  - [50] Shuran Song, Samuel P Lichtenberg, and Jianxiong Xiao. Sun rgb-d: A rgb-d scene understanding benchmark suite. In *Proceedings of the IEEE conference on computer vision and pattern recognition*, pages 567–576, 2015.
  - [51] Mikaela Angelina Uy, Quang-Hieu Pham, Binh-Son Hua, Duc Thanh Nguyen, and Sai-Kit Yeung. Revisiting point cloud classification: A new benchmark dataset and classification model on real-world data. In *International Conference on Computer Vision (ICCV)*, 2019.
  - [52] Mikaela Angelina Uy, Quang-Hieu Pham, Binh-Son Hua, Thanh Nguyen, and Sai-Kit Yeung. Revisiting point cloud classification: A new benchmark dataset and classification model on real-world data. In *Proceedings of the IEEE/CVF international conference on computer vision*, pages 1588–1597, 2019.
  - [53] Ashish Vaswani, Noam Shazeer, Niki Parmar, Jakob Uszkoreit, Llion Jones, Aidan N Gomez, Łukasz Kaiser, and Illia Polosukhin. Attention is all you need. In *Advances in neural information processing systems*, pages 5998–6008, 2017.
  - [54] Hanchen Wang, Qi Liu, Xiangyu Yue, Joan Lasenby, and Matt J Kusner. Unsupervised point cloud pre-training via occlusion completion. In *Proceedings of the IEEE/CVF international conference on computer vision*, pages 9782–9792, 2021.
  - [55] Limin Wang, Bingkun Huang, Zhiyu Zhao, Zhan Tong, Yinan He, Yi Wang, Yali Wang, and Yu Qiao. Videomae v2: Scaling video masked autoencoders with dual masking. *arXiv preprint arXiv:2303.16727*, 2023.
  - [56] Yue Wang, Yongbin Sun, Ziwei Liu, Sanjay E Sarma, Michael M Bronstein, and Justin M Solomon. Dynamic graph cnn for learning on point clouds. *Acm Transactions On Graphics (tog)*, 38(5):1–12, 2019.
  - [57] Ziyi Wang, Xumin Yu, Yongming Rao, Jie Zhou, and Jiwen Lu. P2p: Tuning pre-trained image models for point cloud analysis with point-to-pixel prompting. *arXiv preprint arXiv:2208.02812*, 2022.
  - [58] Zhirong Wu, Shuran Song, Aditya Khosla, Fisher Yu, Linguang Zhang, Xiaoou Tang, and Jianxiong Xiao. 3d shapenets: A deep representation for volumetric shapes. In *Proceedings of the IEEE conference on computer vision and pattern recognition*, pages 1912–1920, 2015.
  - [59] Saining Xie, Jiatao Gu, Demi Guo, Charles R Qi, Leonidas Guibas, and Or Litany. Pointcontrast: Unsupervised pre-training for 3d point cloud understanding. In *Computer Vision—ECCV 2020: 16th European Conference, Glasgow, UK, August 23–28, 2020, Proceedings, Part III 16*, pages 574–591. Springer, 2020.
  - [60] Le Xue, Mingfei Gao, Chen Xing, Roberto Martín-Martín, Jiajun Wu, Caiming Xiong, Ran Xu, Juan Carlos Niebles, and Silvio Savarese. Ulip: Learning unified representation of language, image and point cloud for 3d understanding. *arXiv preprint arXiv:2212.05171*, 2022.
  - [61] Yaoqing Yang, Chen Feng, Yiru Shen, and Dong Tian. Foldingnet: Point cloud auto-encoder via deep grid deformation. In *Proceedings of the IEEE conference on computer vision and pattern recognition*, pages 206–215, 2018.
  - [62] Li Yi, Vladimir G Kim, Duygu Ceylan, I-Chao Shen, Mengyan Yan, Hao Su, Cewu Lu, Qixing Huang, Alla Sheffer, and Leonidas Guibas. A scalable active framework for region annotation in 3d shape collections. *ACM Transactions on Graphics (ToG)*, 35(6):1–12, 2016.
  - [63] Lantao Yu, Weinan Zhang, Jun Wang, and Yong Yu. Seqgan: Sequence generative adversarial nets with policy gradient. In *Proceedings of the AAAI conference on artificial intelligence*, volume 31, 2017.
  - [64] Xumin Yu, Lulu Tang, Yongming Rao, Tiejun Huang, Jie Zhou, and Jiwen Lu. Point-bert: Pre-training 3d point cloud transformers with masked point modeling. In *Proceedings of the IEEE/CVF Conference on Computer Vision and Pattern Recognition*, pages 19313–19322, 2022.
  - [65] Xiaohua Zhai, Alexander Kolesnikov, Neil Houlsby, and Lucas Beyer. Scaling vision transformers. In *Proceedings of the IEEE/CVF Conference on Computer Vision and Pattern Recognition*, pages 12104–12113, 2022.
  - [66] Renrui Zhang, Ziyu Guo, Peng Gao, Rongyao Fang, Bin Zhao, Dong Wang, Yu Qiao, and Hongsheng Li. Point-m2ae: multi-scale masked autoencoders for hierarchical point cloud pre-training. *arXiv preprint arXiv:2205.14401*, 2022.
  - [67] Zaiwei Zhang, Rohit Girdhar, Armand Joulin, and Ishan Misra. Self-supervised pretraining of 3d features on any point-cloud. In *Proceedings of the IEEE/CVF International Conference on Computer Vision*, pages 10252–10263, 2021.